Korean J. Chem. Eng., **21**(6), 1183-1192 (2004)

Comparison of the Adsorption Dynamics of Air on Zeolite 5A and Carbon Molecular Sieve Beds

Jeong-Geun Jee, Sang-Jin Lee and Chang-Ha Lee†

Department of Chemical Engineering, Yonsei University, Shinchon-dong, Seodaemun-gu, Seoul 120-749, Korea
(*Received 7 April 2004 • accepted 8 July 2004*)

Abstract−Adsorption and desorption in zeolite 5A and CMS beds were compared by using a ternary mixture (N_2/O_2/Ar; 78 : 21 : 1 vol%). Because the breakthrough curves for both beds show a tail by temperature variance, a non-isothermal mathematical model was applied to the simulation of adsorption dynamics. The LDF model with a constant rate parameter was enough to predict the experimental breakthrough and temperature curves of an equilibrium separation bed, while the modified LDF model with a concentration-dependent parameter should be applied to a kinetic separation bed. In the CMS bed initially saturated with He, Ar was the first breakthrough component with N_2 following after a short interval. Then, after a long interval, the breakthrough of O_2 occurred with a broad roll-up due to its fast diffusion rate and the relatively slow diffusion rate of N_2. In the CMS bed initially saturated with O_2, the breakthrough curves of O_2 and N_2 showed a very broad shape because of the slow diffusion of N_2 into CMS. In the zeolite 5A bed, the breakthrough time sequence was Ar, O_2, and N_2 at very close time intervals. After the sharp roll-ups of O_2 and Ar, the variation of the breakthrough curves was negligible. The inflection of the temperature profile in the zeolite 5A bed was caused by the crossover of the O_2 and N_2 MTZs, while in the CMS bed it was caused by the difference in the diffusion rates of O_2 and N_2.

Key words: Adsorption Dynamics, Air, Ternary Mixture, CMS, Zeolite 5A, Roll-up, Thermal Effect

INTRODUCTION

The separation and purification of O_2, N_2, and Ar from ambient air by using zeolite and carbon molecular sieve (CMS) are of considerable interest to numerous chemical and petrochemical industries. Indeed, pressure or vacuum swing adsorption (PSA or VSA) processes using these adsorbents have been extensively studied in the industry to obtain a desired product [Ahn et al., 2001; Yang, 1987].

In the field of air separation, various zeolites are generally used to produce O_2 from air while CMS is used to produce high purity N_2 [Jee et al., 2001; Sircar and Hanley, 1993; Mendes et al., 2000; Budner et al., 1999]. However, because air also contains a small amount of Ar, which has physical properties similar to those of O_2, zeolite bed product contains a substantial amount of impurity in the form of Ar [Rege and Yang, 2000]. That is, the upper limit of O_2 purity is restricted to less than 95% in an equilibrium separation process using zeolite. To overcome this limitation and produce O_2 with a high purity level of over 99%, a CMS bed was used as an additional purifier for minor impurities contained in product from the zeolite process such as N_2 and Ar [Rege and Yang, 2000; Jee et al., 2004; Hayashi et al., 1996]. Generally, N_2 acted as a strong adsorbate in zeolite due to its higher equilibrium adsorbed amount, while O_2 was a strong adsorbate in CMS due to its faster diffusion into the adsorbent pore [Yang, 1987; Ruthven, 1994; Jee et al., 2002a]. Zeolite 4A also produces N_2 from ambient air because N_2 acts as a weak adsorbate due to its slow diffusion rate on the adsorbent pellet [Ahn and Lee, 2002; Farooq et al., 1993]. Therefore, high purity O_2 and N_2 can be produced from a well designed kinetic separation process combined with an equilibrium separation process.

Prior to designing the cyclic adsorption process, it is crucial to understand the dynamic characteristics of each adsorption bed in order to achieve a high working capacity for a given adsorbent and improve process efficiency. With regard to air separation systems using adsorption technology, adsorbents have been widely studied in terms of adsorption isotherms, especially adsorption selectivity. However, to select the most appropriate adsorbent for the specific processes, it is necessary to consider the adsorption dynamics of each adsorbent bed [Choi et al., 2003; Kim et al., 2002].

In this study, the adsorption dynamics of air on each fixed bed packed with a single adsorbent such as zeolite 5A and CMS was studied by using a ternary mixture (N_2/O_2/Ar, 78 : 21 : 1 vol%) as dried air. The adsorption characteristics of both beds, such as breakthrough time, breakthrough shape, thermal effect due to the heat of adsorption, and heat exchange between the adsorption bed and its surroundings were theoretically and experimentally compared. In addition, the effect of the initial condition of the bed on the resulting dynamics was investigated by using pure He and O_2. A non-isothermal mathematical model incorporating mass, energy and momentum balances was used for the simulation of the adsorption dynamics [Park, 2002]. The modified LDF model considers the concentration-dependent diffusivity applied to the dynamics of the CMS bed, while the general LDF model considers the constant diffusion rate in the zeolite 5A bed. Results of the adsorption dynamics can be used in the design of the cyclic process in O_2 PSA, O_2 purification, N_2 PSA, etc.

EXPERIMENTAL

A ternary mixture (N_2/O_2/Ar; 78 : 21 : 1 vol%, DaeSung Industrial Gas) was used as a feed gas for the breakthrough experiments. As an initial condition, the breakthrough experiments were conducted with

†To whom correspondence should be addressed.
E-mail: leech@yonsei.ac.kr

Table 1. Operating conditions for breakthrough experiments

Adsorbent	Bed initial condition	Run no.	Adsorption pressure [atm]	Feed flow rate [LSTP/min]
CMS	He saturated	Run 1	5.8	2
		Run 2		4
		Run 3		6
		Run 4	4.35	2
		Run 5		4
		Run 6		6
	O_2 saturated	Run 7	5.8	2
		Run 8		4
		Run 9		6
		Run 10	4.35	2
		Run 11		4
		Run 12		6
Zeolite 5A	He saturated	Run 13	5.8	2
		Run 14		4
		Run 15		6
		Run 16	4.35	2
		Run 17		4
		Run 18		6

the beds saturated by either pure O_2 (99.9+%) or He (99.99+%) and with each under the same experimental pressure. The operating pressure was in the range of 4.35 and 5.8 atm and the feed flow rate was in the range of 2 to 6 LSTP/min. Feed temperature was in the range of 300 K to 302 K depending on room temperature. More detailed experimental conditions are shown in Table 1.

A schematic diagram of the breakthrough apparatus is shown in Fig. 1. The adsorption bed was made of stainless-steel pipe with a length of 100 cm, an ID of 3.6 cm, and a wall thickness of 1.75 mm. Four resistance temperature detectors (RTD, Pt 100 Ω) were installed at the positions of 10, 30, 50, and 75 cm from the feed end

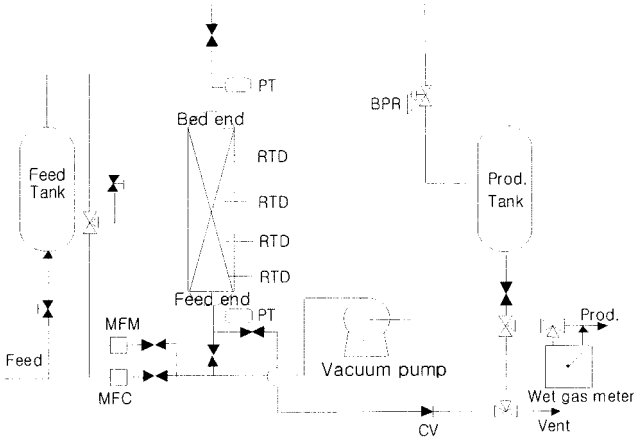

Fig. 1. Schematic diagram of apparatus for breakthrough experiment.
MFC: Mass Flow Controller
MFM: Mass Flow Meter
PT: Pressure Tranducer
BPR: Back Pressure Regulator
RTD: Resistance Temperature Detector
CV: Check Valve

Table 2. Characteristics of adsorbents and adsorption bed

Properties	Adsorbents	
	Zeolite 5A	CMS
Type	Sphere	Sphere
Average pellet radius, R_p [cm]	0.157	0.115
Bed density, ρ_B [g/cm^3]	0.795	0.820
Pellet density, ρ_p [g/cm^3]	1.16	1.1
Heat capacity, C_{ps} [cal/g·K]	0.22	0.27
Bed porosity, ε [-]	0.314	0.255
Adsorption bed		
Length, L [cm]		100
Inside radius, R_{Bi} [cm]		1.7
Outside radius, R_{Bo} [cm]		1.875
Heat capacity of column, C_{pw} [cal/g·K]		0.12
Density of column, ρ_w [g/cm^3]		7.83
Internal heat transfer coefficient, h_i [cal/cm^2·K·sec]		9.2E-4
External heat transfer coefficient, h_o [cal/ cm^2·K·sec]		3.4E-4

to measure the temperature variations inside the bed. The flow rate was controlled by a mass flow controller and the total amount of feed flow was measured by a wet gas meter (Sinagawa Co.). In order to keep the pressure in the adsorption bed constant, an electric back pressure regulator was installed between the adsorption bed and the product bed. The experimental pressure was measured by two pressure transducers equipped at the top and bottom of the bed.

The concentration of the influent and effluent was analyzed by a mass spectrometer (Balzers, QME 200). This analyzer was confirmed by a gas chromatography (HP, 5890II). The system was fully automated by a personal computer with a developed control program, and all measurements including flow rate, pressure, temperature, and concentration were saved on the computer through an AD converter. The characteristics of adsorbents and adsorption beds are listed in Table 2.

MATHEMATICAL MODEL

To understand the dynamic behaviors of each adsorption bed, the mathematical models were developed on the basis of the following assumptions: (i) the gas phase behaves as an ideal gas mixture, (ii) radial concentration and temperature gradients are negligible, (iii) thermal equilibrium between adsorbents and bulk flow is assumed, (iv) the flow pattern is described by the axially dispersed plug flow model, and (v) the pressure drop along the bed is considered by using the Ergun equation. The assumption of neglecting radial gradient was widely accepted by numerous adsorption studies [Rota and Wankat, 1990; Jee et al., 2002b; Kim et al., 2004].

The component and overall mass balances for the bulk phase in the adsorption column are given by

$$-D_L\frac{\partial^2 C_i}{\partial z^2}+\frac{\partial(uC_i)}{\partial z}+\frac{\partial C_i}{\partial t}+\rho_p\left(\frac{1-\varepsilon}{\varepsilon}\right)\frac{\partial \overline{q}_i}{\partial t}=0 \quad (1)$$

$$\frac{\partial(uC)}{\partial z}+\frac{\partial C}{\partial t}+\rho_p\left(\frac{1-\varepsilon}{\varepsilon}\right)\sum_{i=1}^{n}\frac{\partial \overline{q}_i}{\partial t}=0 \quad (2)$$

Applying ideal gas law (C_i=Py_i/RT and C=P/RT) to Eqs. (1) and

(2), the component and overall mass balances can be represented as follows:

$$-D_L\frac{\partial^2 y_i}{\partial z^2}+\frac{\partial(uy_i)}{\partial z}+\frac{\partial y_i}{\partial t}+\rho_p\frac{RT}{P}\left(\frac{1-\varepsilon}{\varepsilon}\right)\frac{\partial \bar{q}_i}{\partial t}=0 \tag{3}$$

$$\frac{\partial P}{\partial t}+P\frac{\partial u}{\partial z}+u\frac{\partial P}{\partial z}+PT\left[\frac{\partial}{\partial t}\left(\frac{1}{T}\right)+u\frac{\partial}{\partial z}\left(\frac{1}{T}\right)\right]+\rho_p RT\left(\frac{1-\varepsilon}{\varepsilon}\right)\sum_{i=1}^{n}\frac{\partial \bar{q}_i}{\partial t}=0 \tag{4}$$

Another characteristic of the adsorption process is the temperature variation caused by the heat of adsorption and desorption [Park et al., 2002]. In this study, since the range of temperature variation during the cyclic operation was about 3 to 10 K, a themal effect on the total cyclic performance was considered to minimize the deviation.

The energy balance for the gas phase also includes the heat transfer to the column wall.

$$-K_L\frac{\partial^2 T}{\partial z^2}+\varepsilon\rho_p C_{pg}\left(u\frac{\partial T}{\partial z}+T\frac{\partial u}{\partial z}\right)+(\varepsilon_t\rho_g C_{pg}+\rho_B C_{ps})\frac{\partial T}{\partial t}-\rho_B(-\Delta\bar{H}_i)\sum_{i=1}^{n}\frac{\partial \bar{q}_i}{\partial t}+\frac{2h_i}{R_{Bi}}(T-T_w)=0 \tag{5}$$

Where, ε_t is the total void fraction ($=\varepsilon+(1-\varepsilon)\alpha$), and ρ_B is the bed density, ($=(1-\varepsilon)\rho_p$).

In order to consider the heat loss through a wall and the heat accumulation in the wall, another energy balance for the wall of the adsorption bed was used.

$$\rho_w C_{pw}A_w\frac{\partial T_w}{\partial t}=2\pi R_{Bi}h_i(T-T_w)-2\pi R_{Bo}h_o(T_w-T_{atm}) \tag{6}$$

where, $A_w=\pi(R_{Bo}^2-R_{Bi}^2)$

The boundary and initial conditions of mass and energy balances are presented below. The well-known Danckwerts boundary conditions were applied [Yang and Lee, 1998a].

<Boundary conditions>

$$-D_L\left(\frac{\partial y_i}{\partial z}\right)\Big|_{z=0}=u(y_i|_{z=0^-}-y_i|_{z=0^+});\ \left(\frac{\partial y_i}{\partial z}\right)\Big|_{z=L}=0 \tag{7a}$$

$$-K_L\left(\frac{\partial T}{\partial z}\right)\Big|_{z=0}=\rho_g C_{pg}u(T|_{z=0^-}-T|_{z=0^+});\ \left(\frac{\partial T}{\partial z}\right)\Big|_{z=L}=0 \tag{7b}$$

Where, $y_i|_{z=0^-}$ means feed composition for component i.

<Initial condition for fluid flow>

$$c_i(z,0)=c_0;\ \bar{q}_i(z,0)=q_i^* \tag{8}$$

<Initial condition for heat flow>

$$T(z,0)=T_{atm} \tag{9}$$

In this study, the adsorption beds were initially saturated with pure O_2 or He under the same adsorption pressure.

To consider the pressure drop effect across the bed, Ergun's equation was introduced as a momentum balance [Yang et al., 1998b].

$$-\frac{dP}{dz}=a\mu u+b\rho u|u| \tag{10a}$$

$$a=\frac{150}{4R_p^2}\frac{(1-\varepsilon)^2}{\varepsilon^2},\ b=1.75\frac{(1-\varepsilon)}{2R_p\varepsilon} \tag{10b}$$

where u is the interstitial velocity.

The multi-component adsorption equilibrium was predicted by the following Langmuir-Freundlich (L-F) model:

<Langmuir-Freundlich isotherm>

$$q_i=\frac{q_{mi}B_iP_i^{ni}}{1+\sum_{j=1}^{n}B_jP_j^{nj}} \tag{11}$$

where, $q_{mi}=k_1+k_2\times T$, $B_i=k_3\exp(k_4/T)$, $n_i=k_5+k_6/T$

In this study, the general LDF model assuming constant diffusivity was applied for the sorption rate of zeolite 5A and the modified LDF model with following concentration-dependent diffusivity for CMS.

<Gluekauf's LDF model for zeolite 5A>

$$\frac{\partial \bar{q}_i}{\partial t}=\omega_i(q_i^*-\bar{q}_i),\ \omega_i=\frac{KD_{ei}}{R_p^2} \tag{12}$$

In this model, the effective diffusivity, D_{ei}, was assumed constant. Because the diffusion time constants of O_2, N_2 and Ar on zeolite 5A showed little concentration dependency, this model was used in the equilibrium separation bed (zeolite 5A).

<Modified LDF model for CMS>

Because the diffusion time constant, D_{ei}/R_p^2, on CMS showed strong dependency on the sorbate concentration, the following structural diffusion model was suggested by Do [1996].

$$D_{ei}\approx\frac{D_{oi}}{dq_i/dP_i} \tag{13}$$

Recently, Bae and Lee [2004] suggested the modified structural diffusion model by using the supercritical relationship.

If this relation is applied to the above structural diffusion model with Langmuir isotherm, the modified model is as follows [Bae et al., 2004].

$$\frac{\partial \bar{q}_i}{\partial t}=\omega_i(q_i^*-\bar{q}_i),\ \omega_i=\frac{KD_{ei}}{R_p^2} \tag{14}$$

Where, $D_{ei}/R_p^2=C\cdot P_r^{0.5}(1+B_iP_i)^2$

The adsorption isotherm and rate parameters of N_2, Ar, and O_2 on CMS and zeolite 5A are presented in Table 3. And these values were very similar to the published data [Ruthven et al., 1986; Chen et al., 1994; Sorial et al., 1983; Miller et al., 1987].

RESULTS AND DISCUSSION

1. The Adsorption Dynamics of CMS Bed

The breakthrough curves for N_2, O_2, and Ar on the CMS bed are shown in Fig. 2. As an initial condition, He, non-adsorptive, was used to pressurize the bed to adsorption pressure. As shown in this figure, Ar was the first breakthrough component at about 110 sec, followed by N_2 at very close intervals of about 5-10 sec each. In particular, the breakthrough curve for N_2 was very steep and showed little tailing, while that of Ar was relatively broad and showed a small excursion. At the N_2 plateau, N_2 concentration increased slightly with time until the breakthrough of the Ar had finished. Then, it began to decrease with a tail at the beginning of the breakthrough of the O_2. The breakthrough of the O_2 appeared at about 250 sec, showing the weak roll-up phenomenon.

Table 3. LRC parameters and rate coefficients for zeolite 5A and CMS

Adsorbent	Adsorbate	k_1*10^3 (mol/g)	k_2*10^6 (mol/g·K)	k_3*10^4 (1/atm)	k_4 (K)	k_5 (−)	k_6 (K)	Diffusion rate constants* (D_{ei}/R_p^2)
CMS	N_2	23.63	−63.80	659.0	49.65	1.692	−270.0	0.000047
	O_2	15.27	−32.30	22.90	966.1	1.187	−106.0	0.024
	Ar	20.42	−53.00	239.7	324.6	1.646	−238.2	0.00009
Zeolite 5A	N_2	6.210	−12.70	1.986	1970	2.266	−396.5	0.0066
	O_2	7.151	−18.20	54.19	662.6	−1.101	656.4	0.0267
	Ar	7.151	−18.20	54.19	662.6	−1.101	656.4	0.0267

*Diffusion rate constants in CMS bed mean C.

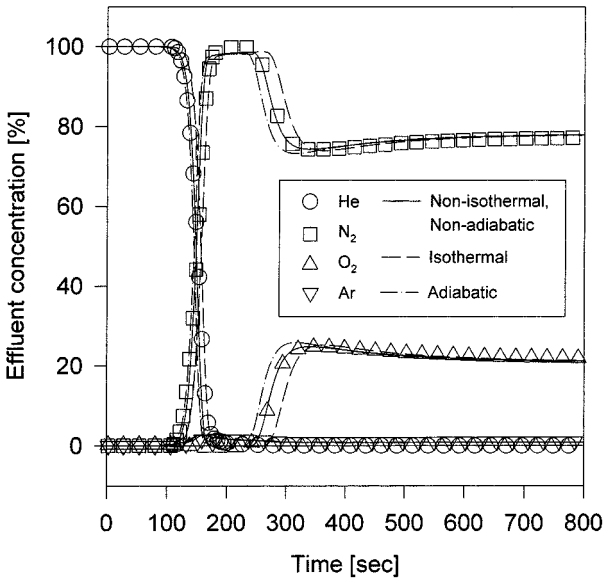

Fig. 2. Experimental and simulated concentration breakthrough curves at 5.8 atm adsorption pressure and 4 LSTP/min feed flow rate (adsorption bed was initially saturated with He at 5.8 atm and 300.5 K) in the CMS bed.

The roll-up phenomenon generally occurs when the weakly adsorbed components lose their adsorption sites due to the competitive adsorption of more strongly adsorbed components, which follow the preceding wavefronts of weakly adsorbed components [Yand and Lee, 1998a; Huang and Fair, 1988; Chlendi and Tondeur, 1995]. However, it is well known that the equilibrium selectivity of O_2, N_2 and Ar on CMS is negligible; and the partial pressure of N_2 in the feed is much higher than that of the others. Thus, the roll-up phenomena in the CMS bed mainly stemmed from the great difference in the diffusion rates of the O_2 and N_2/Ar.

To investigate the thermal effect on the adsorption dynamics in the CMS bed, the simulated breakthrough curves under non-isothermal/non-adiabatic, isothermal, and adiabatic conditions were compared, as shown in Fig. 2. As can be seen, the isothermal and adiabatic conditions deviated somewhat from the experimental result. Therefore, an energy balance is strongly recommended in order to design a PSA process for air separation accurately. More details on the thermal dynamics involved are presented in Figs. 3 and 4.

Temperature variations with time at four locations around the CMS bed are presented in Fig. 3. Temperature excursion was about 6-8 K and the temperature profile showed a long tail. This led to small concentration variation in the breakthrough curves of O_2 and N_2,

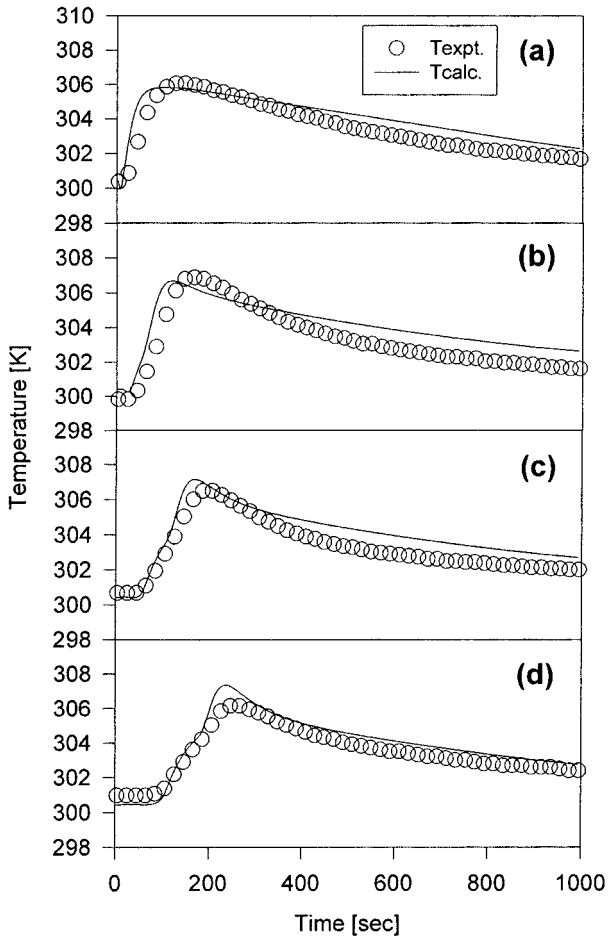

Fig. 3. Temperature variation curves at the position of (a) 10, (b) 30, (c) 50, and (d) 75 cm from the feed inlet at 5.8 atm adsorption pressure and 4 LSTP/min feed flow rate (adsorption bed was initially saturated with He at 5.8 atm and 300.5 K) in the CMS bed.

as shown in Fig. 2. The temperature profile for the feed end showed a steeper increase than in the vicinity of the product end because O_2, the strong adsorbate in CMS, was preferentially adsorbed near the feed end. However, as shown by the temperature profiles in Figs. 3(c) and (d), there was a small inflected increase because of the roll-up of N_2.

To give a clearer insight into the adsorption dynamics of a CMS bed, concentration and temperature profiles in the gas phase at 20, 80, and 220 sec from the beginning of the feed input step are presented in Fig. 4. As can be seen in Fig. 4(a), He was propagated to

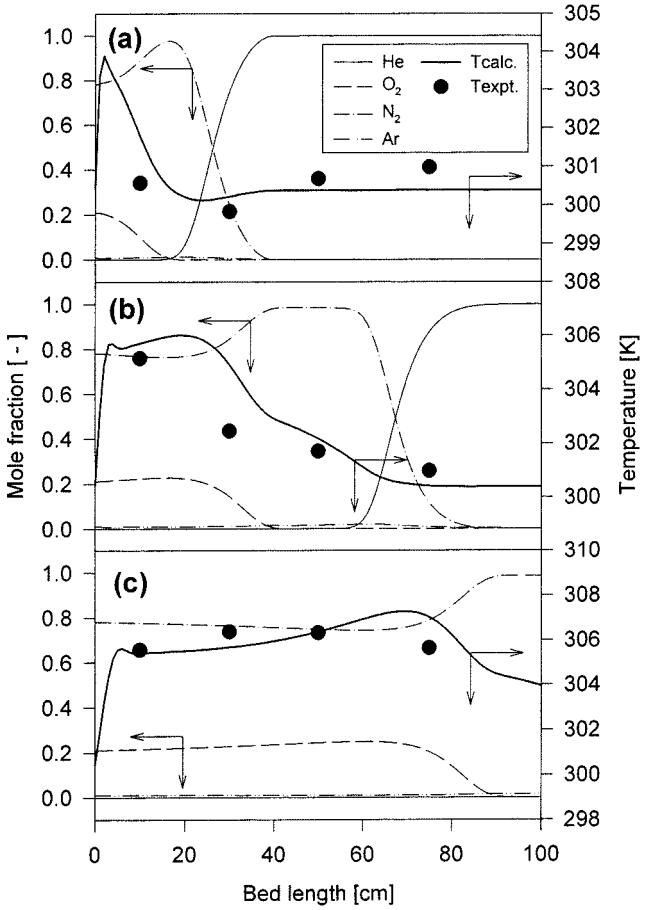

Fig. 4. Concentration and temperature profiles along the bed in the gas phase at (a) 20, (b) 80, and (c) 220 sec at 5.8 atm adsorption pressure and 4 LSTP/min feed flow rate (adsorption bed was initially saturated with He at 5.8 atm and 300.5 K) in the CMS bed.

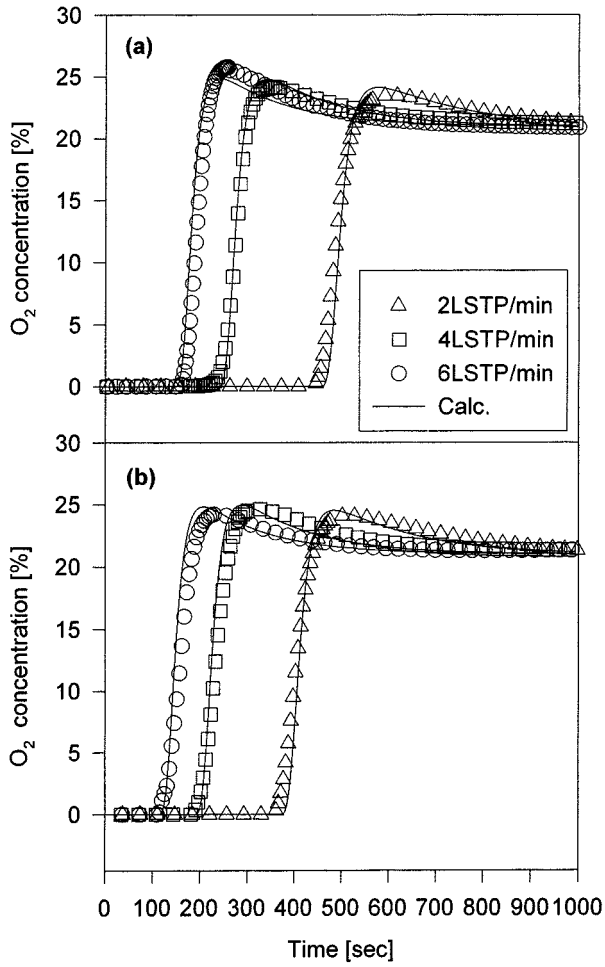

Fig. 5. Effect of feed flow rate on O_2 breakthrough curve at (a) 5.8 and (b) 4.35 atm adsorption pressure (adsorption bed was initially saturated with He at 300.5 K) in the CMS bed.

the bed end with a sharp wave front. And the roll-up of N_2 was shown even at 20 sec in Fig. 4(a) because of the O_2 wave front. Therefore, the temperature sharply increased at the feed inlet because of the adsorption of O_2 while the temperature at the point of the roll-up of N_2 was slightly lower than at the bed end. In Fig. 4(b), the O_2 wave front is shown as a broad roll-up because of the relatively slow adsorption rate and high partial pressure of N_2. The profile of N_2 is shown simultaneously as a broad plateau. And the temperature inflection at 40 cm from the feed end is the result of the separated concentration wave front between the N_2 and O_2. In other words, the steep temperature curvature in the position of 30 to 40 cm from the feed end was due to the O_2 wave front while the broad one in the position of 40 to 60 cm resulted from N_2 adsorption. Next, the small inflection of the temperature wave front after 220 sec was shown near the product end in Fig. 4(c). In Fig. 4, it is evident that the Ar roll-up was small but very wide at the same range of the roll-up of N_2. This is because the desorption rate of Ar is the slowest even though Ar is the first breakthrough component, as indicated in Fig. 2.

Fig. 5 shows the effect of feed flow rate and adsorption pressure on the breakthrough curves of O_2 in the CMS bed. In all of the experimental conditions, the linear increase of the feed flow rate did not cause a linear decrease of breakthrough time because the loading amount is limited by a mass transfer resistance into the pellet under fast flow rate conditions. Indeed, the shape and slope of the breakthrough curves did not noticeably change despite a variation of flow rates. Although the adsorption pressure decreased from 5.8 atm to 4.35 atm, the breakthrough time did not severely decrease. This was because the adsorption dynamics were dominated by the kinetic effect instead of the equilibrium effect. Furthermore, a roll-up and long tailing of the O_2 breakthrough curves under all conditions were observed even though the O_2 acted as the strongest adsorbate and was the last breakthrough component in the CMS bed. As shown in Fig. 4 and Table 3, this stemmed from the slower diffusion rate of N_2 and the effect of heat of adsorption.

In the instance of O_2 saturation as an initial condition, the breakthrough curves of N_2, O_2, and Ar on the CMS bed are shown in Fig. 6. Differing from the results in Fig. 2, the concentrations of O_2 and N_2 slowly approached their input concentrations with a very broad slope and tailing, while the breakthroughs of the N_2 and Ar were shown to take place an earlier period of time. Most of the N_2 and Ar were not adsorbed because of their slow diffusion rate - in comparison with O_2 - into the CMS bed.

It is noteworthy that the simulated results under three different thermal conditions showed negligible differences, as shown in Fig.

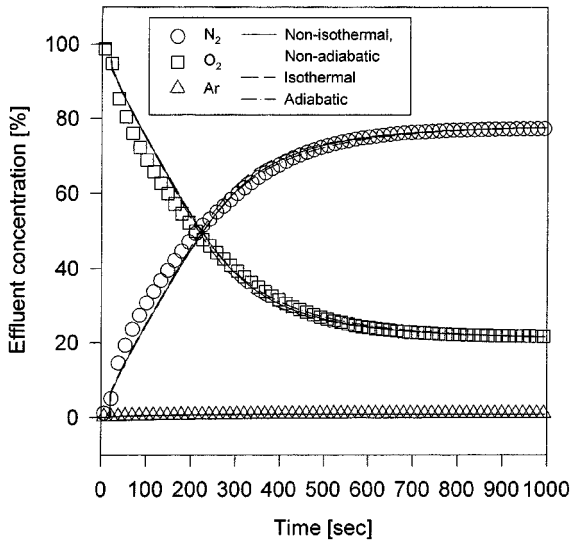

Fig. 6. Experimental and simulated concentration breakthrough curves at 5.8 atm adsorption pressure and 4 LSTP/min feed flow rate (adsorption bed was initially saturated with O_2 at 5.8 atm and 302 K) in the CMS bed.

6, a different outcome from what is seen in Fig. 2. As shown in Fig. 7, the temperature variations with time decreased within 2-4 K within a short period of time due to the desorption of O_2. Furthermore, the variation in the temperature profile decreased along the bed and the temperature recovered relatively quickly to the level of the inlet temperature, as opposed to the results in Fig. 3. This implies that the thermal effect is not noticeable in this system because the heat of adsorption by feed gas offsets the heat of desorption by initially saturated O_2.

The concentration and temperature profiles at 20, 200, and 500 sec from the beginning of the feed input step are presented in Fig. 8. As can be seen in Fig. 8(a), the MTZ's of the N_2 and O_2 proceeded to the product end at the early breakthrough time of about 20 sec. N_2 adsorbed little in solid phase because of its relatively slow diffusion rate while O_2 was mainly desorbed at the feed end. However, since the velocity of the N_2 MTZ was very slow, as shown in Fig. 8(b), the concentration wave front of the N_2 could not entirely pass the adsorption bed, even after about 200 sec. Furthermore, the temperature profile showed a concave shape for temperature in the bed after a sharp increase of temperature at the feed end because of the adsorption of N_2 in the bed. As shown in Fig. 8(c), even though a relatively long time (about 500 sec) passed, the temperature was

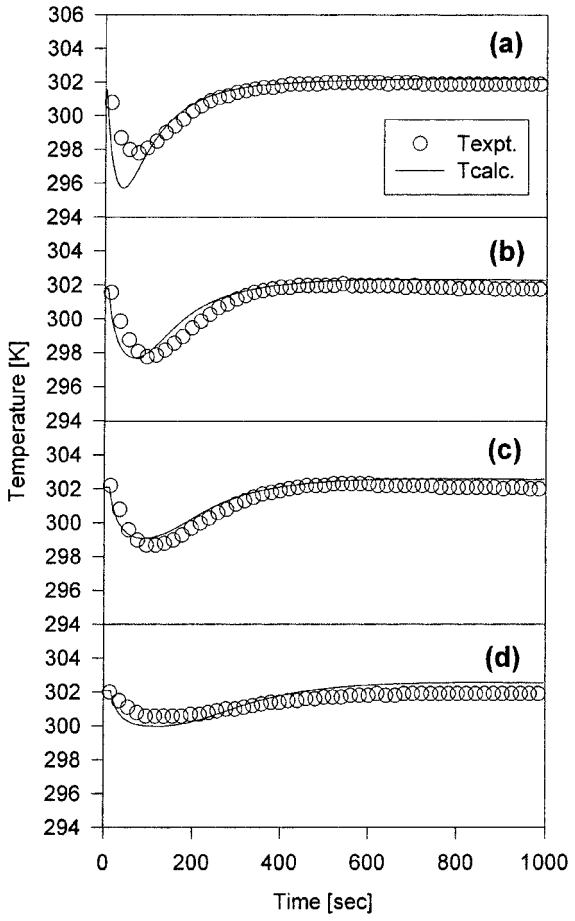

Fig. 7. Temperature variation curves at the position of (a) 10, (b) 30, (c) 50, and (d) 75 cm from the feed inlet at 5.8 atm adsorption pressure and 4 LSTP/min feed flow rate (adsorption bed was initially saturated with O_2 at 5.8 atm and 302 K) in the CMS bed.

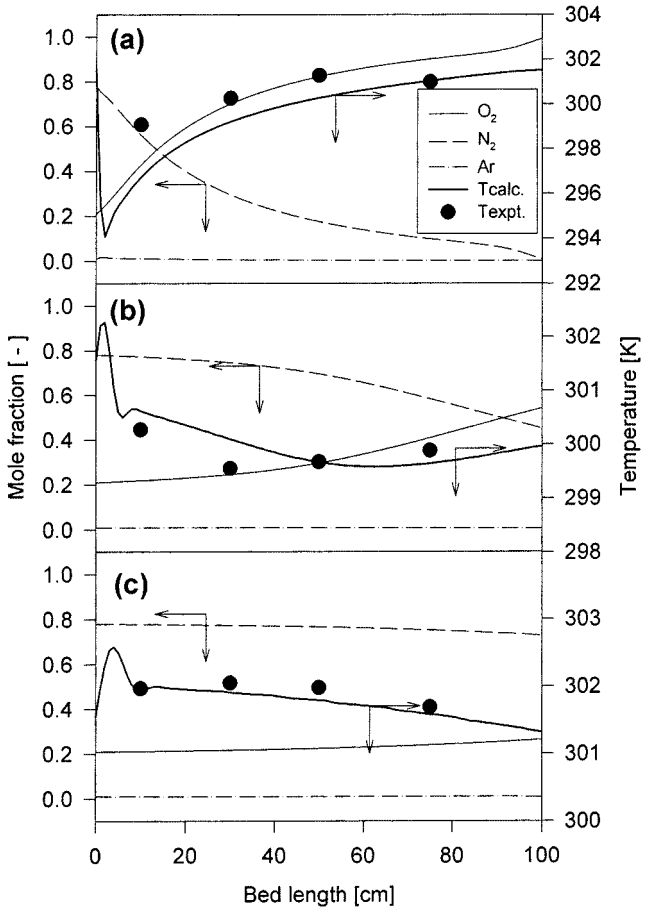

Fig. 8. Concentration and temperature profiles along the bed in the gas phase at (a) 20, (b) 200, and (c) 500 sec at 5.8 atm adsorption pressure and 4 LSTP/min feed flow rate (adsorption bed was initially saturated with O_2 at 5.8 atm and 302 K) in the CMS bed.

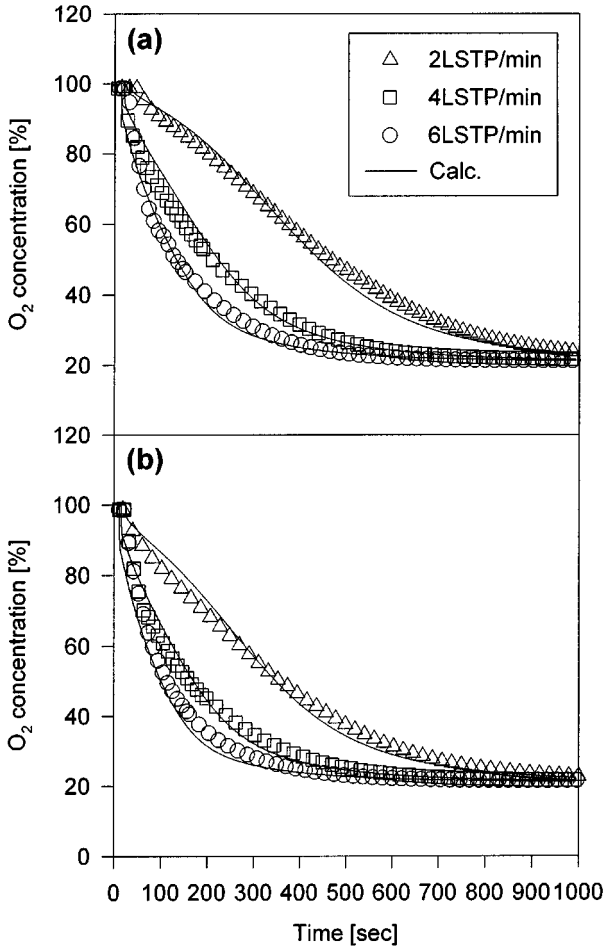

Fig. 9. Effect of feed flow rate on O_2 breakthrough curve at (a) 5.8 and (b) 4.35 atm adsorption pressure (adsorption bed was initially saturated with O_2 at 302 K) in the CMS bed.

linear but slightly decreased toward the product end because the adsorption of N_2 and desorption of O_2 were in progress.

Fig. 9 shows the effect of the feed flow rate and the adsorption pressure on the breakthrough curves of O_2 with regard to the O_2 saturated bed. The breakthrough time was lengthened by a decrease in the feed flow rate. As with the results in Fig. 5, the linear increase in the feed flow rate did not lead to a linear decrease of breakthrough time. In addition, the effect of adsorption pressure on the breakthrough curves was not significant although the breakthrough time slightly decreased and its curvature is seen to be slightly steeper. However, unlike the results from an He saturated condition, the smaller the feed flow rate, the longer the tailing and the broader the breakthrough curves.

2. Adsorption Dynamics of Zeolite 5A Bed

Fig. 10 shows the breakthrough curves of air for the He saturated zeolite 5A bed. This figure shows that the initial saturation He was completely vented as soon as the simultaneous breakthrough of O_2 and Ar occurred. Furthermore, the breakthrough of N_2 followed at a short interval of about 10 sec. Compared with the difference between the breakthrough times of O_2 and N_2 in the CMS bed, as shown in Fig. 2, the difference between breakthrough times was not prominent for the zeolite 5A bed. The velocity of the N_2 MTZ

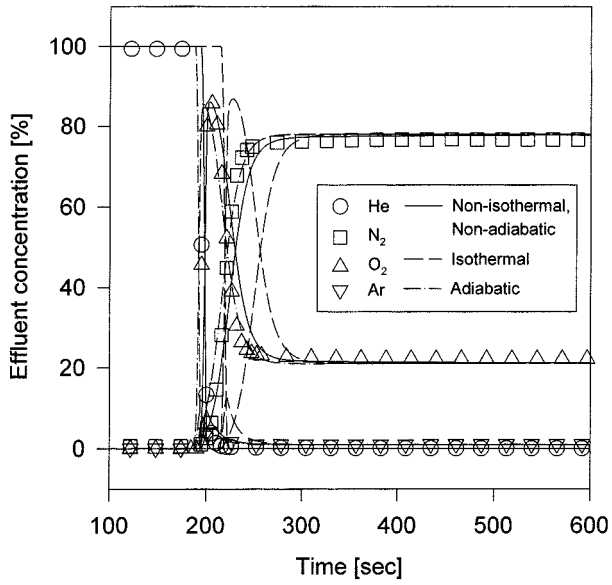

Fig. 10. Experimental and simulated concentration breakthrough curves at 5.8 atm adsorption pressure and 4 LSTP/min feed flow rate (adsorption bed was initially saturated with He at 5.8 atm and 300.5 K) in the zeolite 5A bed.

was fairly fast because the concentration of N_2 in the feed was relatively high regardless of its high adsorption capacity. Also, sharp roll-ups of O_2 and Ar were observed due to the strong adsorption of N_2. However, after the breakthrough of N_2, at 300 sec, the variation in all of the curves was relatively small compared with the results from the CMS bed.

Unlike the CMS bed results in Fig. 2, the simulated results for the isothermal condition showed a large deviation in the prediction of the breakthrough curves while the adsorption dynamics seemed to follow a near adiabatic behavior. However, the height of O_2 concentration was similar at three different thermal conditions while the roll-up of O_2 was broad in the case of the isothermal condition and narrow in the case of the adiabatic condition. Furthermore, Ar concentration was also the highest under isothermal conditions.

As shown in Fig. 11, the temperature increment in the zeolite 5A bed was steeper and substantially greater at all positions than in the CMS bed due to the heat of adsorption of the N_2 with highest concentration in the feed. However, as with the CMS bed, a small inflection appeared at 50 and 75 cm from the feed end, as shown in Figs. 11(c) and (d). Even after 1,000 sec, the temperature still had not reached the level of the inlet temperature because of the slow heat exchange between the inner bed and its surroundings.

In Fig. 12, the concentration wave fronts in the zeolite 5A bed are presented along with the temperature profile. As can be seen in Fig. 12(a), the concentration wave front of the N_2 propagated slightly faster than the others at 20 sec. Also, the MTZs of O_2 and Ar showed a small roll-up at nearly the same position as the temperature excursion due to the adsorption of the N_2. However, Fig. 12(b) shows that after 140 sec the roll-up of the O_2 and Ar became higher. Moreover, since the concentration wave front of the O_2 propagated first, an inflection appeared in the temperature profile at the crossover range of wave fronts. In addition, the velocity of the temperature wave front was similar to that of the concentration wave front.

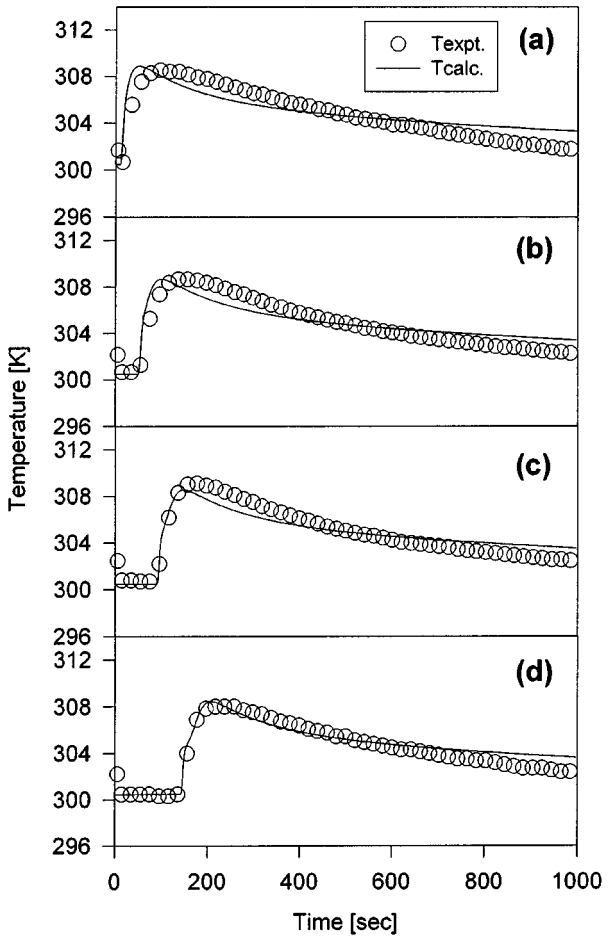

Fig. 11. Temperature variation curves at the position of (a) 10, (b) 30, (c) 50, and (d) 75 cm from the feed inlet at 5.8 atm adsorption pressure and 4 LSTP/min feed flow rate (adsorption bed was initially saturated with He at 5.8 atm and 300.5 K) in the zeolite 5A bed.

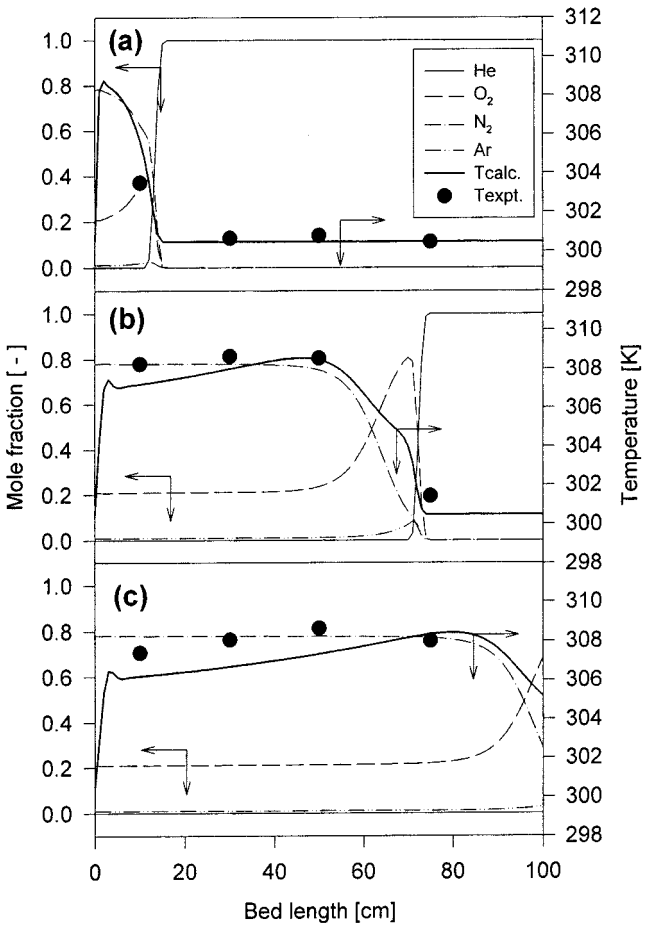

Fig. 12. Concentration and temperature profiles along the bed in the gas phase at (a) 20, (b) 140, and (c) 220 sec at 5.8 atm adsorption pressure and 4 LSTP/min feed flow rate (adsorption bed was initially saturated with He at 5.8 atm and 300.5 K) in the zeolite 5A bed.

As shown in Fig. 12(c), after the initially saturated He was entirely vented, the bed temperature remained almost constant throughout the bed. In contrast to the CMS bed results in Fig. 4, the crossover of the MTZ between O_2 and N_2 did occur in the zeolite 5A bed, but a curvature of the MTZ of O_2 was not observed.

Fig. 13 shows the effect of the feed flow rate and adsorption pressure on the breakthrough curves of O_2 in the zeolite 5A bed. The lower the feed flow rate, the higher the peaks of the O_2 breakthrough curves and the broader the roll-up of O_2. This is because the increased contact time between the adsorbate and adsorbent at a low feed flow rate led to an increase in the net amount of O_2 adsorption on solid phase. Furthermore, in contrast to the results for the CMS bed in Figs. 5 and 9, the effect of adsorption pressure on the breakthrough time was significant in the zeolite 5A bed because the equilibrium selectivity in zeolite 5A was significantly affected by pressure.

CONCLUSIONS

The adsorption dynamics of a ternary mixture [N_2/O_2/Ar, 78 : 21 : 1 vol%] were theoretically and experimentally studied by using equilibrium and kinetic separation beds which were packed with zeolite 5A and CMS, respectively.

In the CMS bed, initially saturated with He, Ar was a first breakthrough component showing a small roll-up and N_2 followed at a very close interval. Then, the breakthrough of O_2 occurred with a broad roll-up due to its fast diffusion rate and the relatively slow diffusion rate of N_2. Since a temperature excursion occurred to within 6-8 K during the breakthrough experiment, the isothermal and adiabatic models led to some deviation in the prediction of the breakthrough curves. In addition, as the MTZ of the O_2 proceeded to the beds end, temperature curves got steeper and a small inflection in the temperature profile was caused by the difference of the diffusion rates of N_2 and O_2 and not by the crossover of MTZ's.

However, in the CMS bed saturated with O_2, the breakthrough curve for the N_2 was very broad because the O_2 acted as a strong adsorbate due to its fast adsorption and desorption rates. Temperature variation was within 2-4 K and the bed temperature recovered to the level of the feed temperature within a short period of time because the heat of desorption of O_2 offset the heat of adsorption of N_2. Consequently, the thermal effect on the breakthrough curves was not noticeable under these conditions. Under both He and O_2 saturation

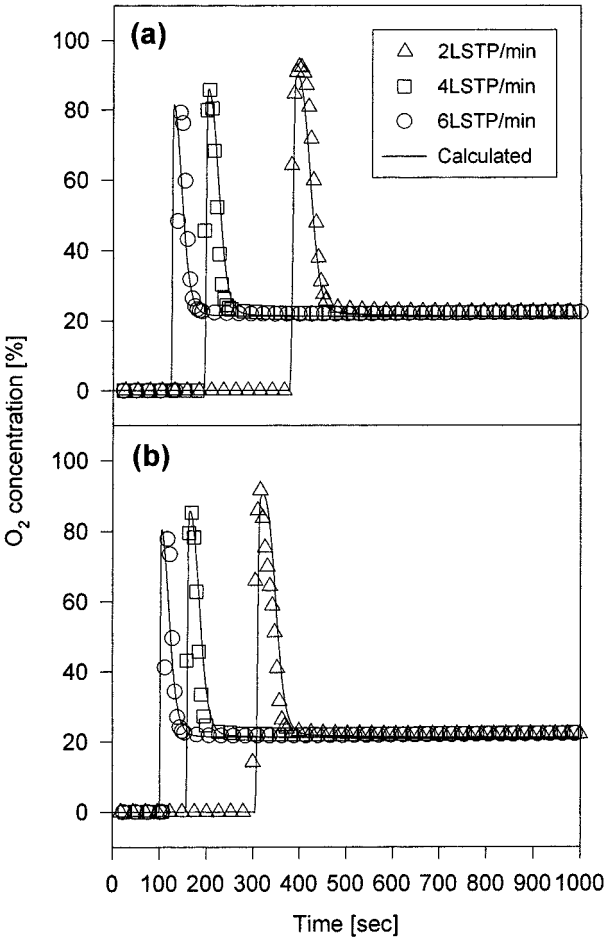

Fig. 13. Effect of feed flow rate on O_2 breakthrough curve at (a) 5.8 and (b) 4.35 atm adsorption pressure (adsorption bed was initially saturated with He at 300.5 K) in the zeolite 5A bed.

conditions, the effect of feed flow rate on the breakthrough curve was significant while that of adsorption pressure was relatively small.

The breakthrough curves of air on the zeolite 5A bed were performed under the condition of He saturation. As a result, the breakthroughs of O_2 and Ar first occurred simultaneously with a sharp roll-up, then the breakthrough of N_2 without a roll-up followed after a very short interval. Since the temperature increased to 8-9 K at all points in the bed, the isothermal model led to a large deviation in prediction results, but the adsorption dynamics showed near adiabatic behaviors. The temperature wave front was steeper than in the CMS and its velocity was almost same as that of the O_2 concentration wave front. In addition, the inflection in the temperature profile was caused by the crossover of the O_2 and N_2 MTZ's. In contrast to the CMS bed, the effects of both feed flow rate and adsorption pressure on the zeolite 5A bed were very significant because of the change of adsorption equilibrium selectivity as well as kinetic selectivity.

ACKNOWLEDGMENT

The financial support of the Carbon Dioxide Reduction and Sequestration R & D Center (C002-0103-001-1-0-0) is gratefully acknowledged.

NOMENCLATURE

A_W : cross sectional area of the wall [cm^2]
B : equilibrium parameter for Langmuir-Freundlich model [atm^{-1}]
C_i : i component concentration in bulk phase [mol/cm^3]
C_{pg}, C_{ps}, C_{pw} : gas, pellet, and wall heat capacity, respectively [cal/g·K]
D_e : effective diffusivity defined by solid diffusion model [cm^2/sec]
D_c : intracrystalline diffusivity [cm^2/sec]
D_L : axial dispersion coefficient [cm^2/sec]
h_i : internal heat transfer coefficient [cal/cm^2·K·sec]
h_o : external heat transfer coefficient [cal/cm^2·K·sec]
$-\Delta\overline{H}$: average heat of adsorption [cal/mole]
k : parameter for LRC model
K : proportionality parameter for LDF model [-]
K_L : axial thermal conductivity [cal/cm·sec·K]
L : bed length [cm]
n : equilibrium parameter for Langmuir-Freundlich model [-]
P : total pressure [atm]
q, q^*, $\overline{q}$: amount adsorbed, equilibrium amount adsorbed and average amount adsorbed, respectively [mol/g]
q_m : equilibrium parameter for Langmuir-Freundlich model [mol/g]
R : gas constant [cal/mol·K]
R_p : radius of pellet [cm]
R_{Bi}, R_{Bo} : inside and outside radius of the bed, respectively [cm]
t : time [sec]
T_{atm} : temperature of atmosphere [K]
T, T_w : pellet or bed temperature and wall temperature, respectively [K]
u : interstitial velocity [cm/sec]
y_i : mole fraction of species i in gas phase [-]
z : axial distance in bed from the inlet [cm]

Greek Letters

α : particle porosity [-]
ε, ε_t : voidage of adsorbent bed and total void fraction, respectively [-]
ρ_g, ρ_p, ρ_B, ρ_w : gas density, pellet density, bulk density and bed wall density, respectively [g/cm^3]
ω : LDF coefficient [sec^{-1}]
θ : dimensionless adsorbed amount [$=q_i/q_{mi}$], [-]
μ : viscosity [g/cm·sec]

Subscripts

B : bed
i : component i
p : pellet
g : gas phase
s : solid
w : wall

REFERENCES

Ahn, H., Yang, J. and Lee, C.-H., "Effects of Feed Composition of Coke Oven Gas on a Layered Bed H_2 PSA Process," *Adsorption*, **7**, 339

(2001).
Ahn, H. and Lee, C.-H., "Sorption Kinetics of N_2, CO and CH_4 on Pelletized Zeolite 4A, 5A and 10X," *J. Chem. Eng. Japan*, **35**, 334 (2002).
Bae, Y. and Lee, C.-H., "Adsorption Equilibria and Kinetics of Eight Pure Gases on a Carbon Molecular Sieve at Elevated Pressure," *Carbon*, **43**, 95 (2004).
Bae, Y., Moon, J. H., Ahn, H. and Lee, C. H., "Effects of Adsorbate Properties on Adsorption Mechanism in a Carbon Molecular Sieve," *Korean J. Chem. Eng.*, **21**, 712 (2004).
Budner, Z., Dula, J., Podstawa, W. and Gawdzik, A., "Study and Modeling of the Vacuum Swing Adsorption (VSA) Process Employed in the Production of Oxygen," *Trans IChemE*, **77**, 405 (1999).
Chen, Y. D., Yang, R. T. and Uawithya, P., "Diffusion of Oxygen, Nitrogen and Their Mixtures in Carbon Molecular Sieve," *AIChE J.*, **40**, 577 (1994).
Chlendi, M. and Tondeur, D., "Dynamic Behavior of Layered Columns in Pressure Swing Adsorption," *Gas Sep. Puri.*, **9**, 231 (1995).
Choi, W. K., Kwon, T. I. and Yeo, Y. K., "Optimal Operation of the Pressure Swing Adsorption (PSA) Process for CO_2 Recovery," *Korean J. Chem. Eng.*, **20**, 617 (2003).
Do, D. D., "A Model for Surface Diffusion of Ethane and Propane in Activated Carbon," *Chem. Eng. Sci.*, **51**, 4145 (1996).
Farooq, S., Rathor, M. N. and Hidajat, K., "A Predictive Model for a Kinetically Controlled Pressure Swing Adsorption Separation Process," *Chem. Eng. Sci.*, **48**, 4129 (1993).
Hayashi, S., Kawai, M. and Kaneko, T., "Dynamics of high Purity Oxygen PSA," *Gas Sep. Puri.*, **10**, 19 (1996).
Huang, C.-C. and Fair, J. R., "Study on the Adsorption and Desorption of Multiple Adsorbates in a Fixed Bed," *AIChE J.*, **34**, 1861 (1988).
Jee, J. G., Kim, M. B. and Lee, C.-H., "Comparison of Pressure Swing Adsorption Processes to Purify Oxygen by Using Carbon Molecular Sieve," *Chem. Eng. Sci.*, **60**(3), in press (2004).
Jee, J.-G., Lee, J.-S. and Lee, C.-H., "Air Separation by a Small-Scale Two-Bed Medical O_2 PSA," *Ind. Eng. Chem. Res.*, **40**, 3647 (2001).
Jee, J. G., Park, M., Yoo, H., Lee, K. and Lee, C.-H., "Adsorption and Desorption Characteristics of Air on Zeolite 5A, 10X, and 13X Fixed Beds," *Sep. Sci. Tech.*, **37**, 3465 (2002a).
Jee, J. G., Park, H., Haam, S. and Lee, C.-H., "Effects of Nonisobaric and Isobaric Steps on O_2 Pressure Swing Adsorption for an Aerator," *Ind. Eng. Chem. Res.*, **41**, 4383 (2002b).
Kim, M.-B., Moon, J.-H. and Lee, C.-H., Oh, M. and Cho, W., "Effect of Heat Transfer on the Transient Dynamics of TSA Process," *Korean J. Chem. Eng.*, **21**, 703 (2004).
Kim, S. J., Cho, S. Y. and Kim, T. Y., "Adsorption of Chlorinated Volatile Organic Compounds in a Fixed Bed of Activated Carbon," *Korean J. Chem. Eng.*, **19**, 61 (2002).
Mendes, Adelio M. M., Costa, Carlos A. V. and Rodrigues, Alirio E., "Analysis of Nonisobaric Steps in Nonlinear Bicomponent Pressure Swing Adsorption Systems. Application to Air Separation," *Ind. Eng. Chem. Res.*, **39**, 138 (2000).
Miller, G. W., Knaebel, K. S. and Ikels, K. G., "Equilibria of Nitrogen, Oxygen, Argon, and Air in Molecular Sieve 5A," *AIChE J.*, **33**, 194 (1987).
Park, C. J., Kim, S. S. and Chun, B. H., "The Heat Transfer Characteristics in Air-Lift Contactor with Activated Carbon for the Separation of Air Pollutants," *Korean J. Chem. Eng.*, **19**, 833 (2002).
Park, I. S., "Numerical Analysis of Fixed Bed Adsorption Kinetics Using Orthogonal Collocation," *Korean J. Chem. Eng.*, **19**, 1001 (2002).
Rege, S. U. and Yang, R. T., "Kinetic Separation of Oxygen and Argon Using Molecular Sieve Carbon," *Adsorption*, **6**, 15 (2000).
Rota, R. and Wankat, P. C., "Intensification of Pressure Swing Adsorption Processes," *AIChE J.*, **36**, 1299 (1990).
Ruthven, D. M., Raghavan, N. S. and Hassan, M. M., "Adsorption and Diffusion of Nitrogen and Oxygen in a Carbon Molecular Sieve," *Chem. Eng. Sci.*, **41**, 1325 (1986).
Ruthven, D. M., "Pressure Swing Adsorption," VCH Publishers (1994).
Sircar, S. and Hanley, B. F., "Fractionated Vacuum Swing Adsorption Process for Air Separation," *Sep. Sci. Tech.*, **28**, 2553 (1993).
Sorial, G. A., Granville, W. H. and Daly, W. O., "Adsorption Equilibria for Oxygen and Nitrogen Gas Mixtures on 5A Molecular Sieves," *Chem. Eng. Sci.*, **38**, 1517 (1983).
Yang, J. and Lee, C.-H., "Adsorption Dynamics of a Layered Bed PSA for H_2 Recovery from Coke Oven Gas," *AIChE J.*, **44**, 1325 (1998a).
Yang, J., Seo, B. K., Baek, K. H., Ko, S.-M. and Lee, C. H., "Effects of Pressure Drop on Non-isothermal PSA Process," *Korean J. Chem. Eng.*, **15**, 211 (1998b).
Yang, R. T., "Gas Separation by Adsorption Processes," Butterworths Publishers (1987).